

Collinear approach for top quark production at ep colliders

G.R.Boroun*

Department of physics, Razi University, Kermanshah 67149, Iran
(Dated: September 16, 2022)

An approximately analysis study of the collinear approach for $t\bar{t}$ production at the Future Circular Collider hadron-electron (FCC-he) and the Large Hadron electron Collider (LHeC) is performed. To study heavy quark production processes, the collinear generalized double asymptotic scaling (DAS) approach in a wide rang of Q^2 is used. The reduced cross sections for top quark pair production at the FCC-he (for $Q^2 \geq m_t^2$) and LHeC (for $Q^2 \leq m_t^2$) center-of-mass energies at the high inelasticity are derived. These results may be considering for both the future collider experiments at center-of-mass energy frontier and the improvement of the phenomenological models on kinematics of low values of the Bjorken variable x . The evolution of the gluon density for heavy-quark production in DIS is obtained at low x to include effects of heavy-quark masses. A nonlinear modification of these results shown that the nonlinear corrections, with respect to the top quark mass, are very small for $Q^2 \propto m_t^2$.

I. Introduction

The Large Hadron electron Collider (LHeC) [1] and the Future Circular Collider hadron-electron (FCC-he) [2] are proposed facilities of using newly built electron-proton center of mass energies at $\sqrt{s} \cong 1.3$ and 3.5 TeV, respectively. At the LHeC and FCC-he, it is foreseen that a 60 GeV electron beam collides with one of the 7 TeV intense proton beams of the LHC, or with a 50 TeV proton beam of a Future Circular Collider for hadron-hadron scattering (FCC-hh). The LHeC and FCC-he measurements can be performed with much increased precision and extended to much lower values of x and high Q^2 . The LHeC provides data on the charm and bottom structure functions extending the range in x, Q^2 by up to 5 or 6 orders of magnitude, respectively, compared to HERA. These new colliders will be devoted to probe the energy frontier and complement the discovery potential of the LHC with measurements of deep inelastic scattering (DIS). The LHeC and FCC-he collisions lead into the region of high parton densities at low x since the kinematic reach goes up to $Q^2 \simeq 1 \text{ TeV}^2$ and $x \simeq 10^{-5} \dots 10^{-6}$ for LHeC and 10^{-7} for FCC-he. These kinematics are pertinent in investigations of lepton-hadron processes at ultra-high energy (UHE) neutrino astroparticle physics [3-4]. Moreover a similar very high energy electron-proton/ion collider (VHEep) [5] has been suggested based on plasma wakefield acceleration, albeit with very low luminosity. The center-of-mass energy, in this collider, is close to 10 TeV which is relevant in investigations of new strong interaction dynamics related to high-energy cosmic rays and gravitational physics. It can be used to study the top-quark physics [6-13]. In particular the LHeC and FCC-he will be provided a

cleaner environment for the study of top quark pair production. The top quark will be produced in these future colliders in pairs ($t\bar{t}$) through quantum chromodynamics (QCD) processes, mostly photon-gluon fusion (PGF) at ultra-high energies $\gamma^* + g \rightarrow t + \bar{t}$. The top quark pair production cross sections are $\sigma_{t\bar{t}} = 984.5 \text{ pb}$ at $\sqrt{s} = 14 \text{ TeV}$ and $\sigma_{t\bar{t}} = 826.4 \text{ pb}$ at $\sqrt{s} = 13 \text{ TeV}$ at CMS [18] and ATLAS [19] respectively. The top quark at the LHC is thereby characterized by final states comprising the decay products of the two W bosons and two b jets, and produced in nuclear collisions with respect to the partonic subprocesses

$$\begin{aligned} q + \bar{q} &\rightarrow t + \bar{t} + X, \\ g + g &\rightarrow t + \bar{t} + X, \\ q + g &\rightarrow t + \bar{t} + X, \end{aligned}$$

where $\sigma_{\text{tot}}^{t\bar{t}}$ can be written as

$$\sigma_{\text{tot}}^{t\bar{t}} = \sum_{ij} \int_0^{4m_t^2/s} d\beta \Phi_{ij}(\beta, \mu_F^2) \hat{\sigma}_{ij}(\beta, m_t, \mu_F^2, \mu_R^2). \quad (1)$$

Here Φ_{ij} is the partonic flux which is a convolution of the densities of partons i, j and $\hat{\sigma}_{ij}$ is the total partonic cross section for the inclusive production of a heavy quark from partons i, j [14-17]. The dimensionless variable $\beta^2 = 1 - \rho$, with $\rho = 4m_t^2/s$, is the squared relative velocity of the final state top quarks having pole mass m_t and produced at the square of the gluonic center of mass energy s . The gluon-gluon fusion (GGF), $g + g \rightarrow t + \bar{t}$, is dominantly at ultra-high energies for $\mu = m_t$, thus partonic cross section is summarized as follows

$$\hat{\sigma}_{gg}(\beta, m_t) = \frac{\alpha_s^2}{m_t^2} \{ f_{gg}^{(0)} + \alpha_s f_{gg}^{(1)} + \alpha_s^2 f_{gg}^{(2)} + \mathcal{O}(\alpha_s^3) \}. \quad (2)$$

The functions f_{gg} are known at leading and high-order approximations and depend only on dimensionless parameters β and ρ [15].

*Electronic address: grboroun@gmail.com; boroun@razi.ac.ir

The total cross section for the single top quark production via charged current (CC) DIS scattering at the LHeC is 1.89 pb [1] due to the center-of-mass energy of 1.3 TeV and at the FCC-he is 15.3 pb [2] due to the center-of-mass energy of 3.5 TeV. It is 0.05 pb [1] for top quark pair production in $t\bar{t}$ photoproduction mode at the LHeC and 1.14 pb at the FCC-he [2]. It means that the top quark with mass about 172.76 ± 0.3 GeV [18] can be studied at future colliders. It derives its mass from its coupling to the Higgs Boson [19]. The $t\bar{t}$ productions at the LHC are implemented and used to extract PDFs [20]. In the future ep collider, top quark pair production via NC ep scattering will be considered. Such future ep collider facilities allow high-precision measurements of certain top quark properties and have high sensitivity in finding new physics beyond the SM.

In this work, in the kinematic regime of the FCC-he, the top quark pair production cross section is calculated in the collinear approach. In sec. II, the theoretical framework for the coefficient function in the collinear approach is presented. In sec. III, the numerical results for the reduced cross section $\sigma_r^{t\bar{t}}(x, Q^2)$ and the ratio $R^{t\bar{t}} = F_L^{t\bar{t}}/F_2^{t\bar{t}}$, in the kinematic regime of the FCC-he, are presented.

II. Theory

The heavy quark pair production at HERA is obtained by fixed number of parton densities (fixed flavour number schemes, FFNS) close to threshold $\mu^2 \sim m_Q^2$ (where m_Q is the heavy quark mass). The resummation of collinear logarithms $\ln(\mu^2/m_Q^2)$ at scales far above the threshold $\mu^2 \gg m_Q^2$ is achieved through the use of variable flavour number schemes (VFNS). When the scale is increased above heavy quark mass thresholds, the number of active flavors increases in VFNS. For realistic kinematics it has to be extended to the case of a general-mass VFNS (GM-VFNS) which is defined similarly to the zero-mass VFNS (ZM-VFNS) in the $Q^2/m_Q^2 \rightarrow \infty$ limit [21,22]. In GM-VFNS the transition, from n_f active flavors to n_f+1 , is considered in the construction of the charm-quark parton distribution function. At some rather large scales (i.e., $Q^2 > m_Q^2$) the transition to two massive quarks (i.e., $n_f \rightarrow n_f + 2$) has been discussed in Refs.[23,24]. In the GM-VFNS at high Q^2 , the heavy-flavor structure functions depend on the active flavor number since here $n_f = 4$ for $m_c^2 < \mu^2 < m_b^2$, $n_f = 5$ for $m_b^2 < \mu^2 < m_t^2$ and $n_f = 6$ for $\mu^2 \geq m_t^2$ is chosen.

Recently in Ref.[25] authors studied the transverse momentum dependent (TMD) gluon distribution function in heavy quark production processes. They used the Kimber-Martin-Ryskin [26] prescription from the Bessel inspired behavior of parton densities at small x . The heavy quark reduced cross section is defined in terms of

the heavy quark structure functions as

$$\sigma_r^{Q\bar{Q}}(x, Q^2) = F_2^{Q\bar{Q}}(x, Q^2) - f(y)F_L^{Q\bar{Q}}(x, Q^2), \quad (3)$$

where $f(y) = y^2/1 + (1-y)^2$ and y is the inelasticity. In the collinear generalized double asymptotic scaling (DAS) [27] approach, the heavy quark structure functions are driven by the following form

$$F_{k=2,L}^{Q\bar{Q}}(x, Q^2) = \sum_{i=g,q,\bar{q}} C_{k,i}^{Q\bar{Q}}(x, \mu^2, m_Q^2) \otimes x f_i(x, \mu^2), \quad (4)$$

where $x f_i$ are the parton distribution functions (PDFs) and $C_{k,i}^{Q\bar{Q}}(x, Q^2)$ are the DIS coefficient functions. The gluon density is dominant for $x < 0.1$, therefore a further simplification with the contribution due to PGF is obtained by neglecting the contributions due to incoming light quarks and antiquarks in Eq. (3), which is justified because they vanish at LO and are numerically suppressed at high order corrections as

$$F_{k=2,L}^{Q\bar{Q}}(x, Q^2) \simeq C_{k,g}^{Q\bar{Q}}(x, \mu^2, m_Q^2) \otimes x f_g(x, \mu^2), \quad (5)$$

where $x f_g(x, Q^2) = G(x, Q^2)$ is the gluon distribution function and the \otimes symbol denotes the convolution integral which turns into a simple multiplication in Mellin N -space. The notation is defined by $a(x) \otimes b(x) = \int_x^1 \frac{dz}{z} a(z) b(\frac{x}{z})$. The coefficient functions at leading-order up to next-to-next-to leading order (NNLO) approximations [25] read

$$\begin{aligned} C_{k,g}^{\text{LO}}(x, \mu^2) &= e_Q^2 a_s(\mu^2) B_{k,g}^{(0)}(x, a), \\ C_{k,g}^{\text{NLO}}(x, \mu^2) &= e_Q^2 a_s(\mu^2) [B_{k,g}^{(0)}(x, a) + a_s(\mu^2) B_{k,g}^{(1)}(x, a)], \\ C_{k,g}^{\text{NNLO}}(x, \mu^2) &= e_Q^2 a_s(\mu^2) [B_{k,g}^{(0)}(x, a) + a_s(\mu^2) B_{k,g}^{(1)}(x, a) \\ &\quad + a_s^2(\mu^2) B_{k,g}^{(2)}(x, a)], \end{aligned} \quad (6)$$

where $a = m^2/Q^2$ and $a_s(\mu^2) = \alpha_s(\mu^2)/4\pi$. The explicit expression for the coefficient function is relegated in Appendix A. The default renormalisation and factorization scales are set to be equal $\mu_R^2 = Q^2 + 4m^2$ and $\mu_F^2 = Q^2$. In order to fix the unphysical mass scale μ , the renormalisation and factorisation scale for the heavy quarks is set to $\mu^2 = Q^2 + 4m^2$. Thereofe, the top quark structure functions at low x are given by the following form

$$F_k^{t\bar{t}}(x, Q^2) = C_{k,g}^{t\bar{t}}(x, \mu^2, m_t^2) \otimes G_{n_f=6}(x, \mu^2), \quad (7)$$

where G_{n_f} is the gluon distribution function due to the number of active quark flavors.

In the presence of heavy quarks, the gluon distribution function $G_{n_f}(x, \mu^2)$ is defined with respect to threshold of heavy quark pair production. In Ref.[28], the authors used a simplified version of the method introduced by Aivazis, Collins, Olness, and Tung (ACOT) [29] using a rescaling variable $x_i = x \eta_i(Q^2)$ where

$i \in u, \bar{u}, d, \bar{d}, s, \bar{s}, c, \bar{c}, b, \bar{b}$ and $\eta_i(Q^2) = 1 + 4M_i^2/Q^2$. The authors of [28] showed that the massless gluon distribution treating active flavor effects properly is defined as

$$G_{n_f=4}(x, Q^2) = \frac{3}{5}G_{n_f=3}(x, Q^2), \quad (8)$$

and

$$G_{n_f=5}(x, Q^2) = \frac{6}{11}G_{n_f=3}(x, Q^2). \quad (9)$$

$G_{n_f=3}(x, Q^2)$ is dependent on $F_2(x, Q^2)$ and $\partial F_2(x, Q^2)/\partial \ln x$ using a Laplace transformation method. Indeed authors in Ref.[28] have demonstrated that a parametrization of the ZEUS experimental data on the proton structure function $F_2(x, Q^2)$ gives an analytic solution for the LO gluon distribution $G_{n_f=3}(x, Q^2)$ as a function of x and Q^2 . This function (i.e., $G_{n_f=3}$) is defined very well for low x ($0 < x \leq 0.06$) by an expression quadratic in both $\ln(Q^2)$ and $\ln(1/x)$ as

$$\begin{aligned} G_{n_f=3}(x, Q^2) = & -2.94 - 0.359\ln(Q^2) - 0.101\ln^2(Q^2) \\ & + (0.594 - 0.0792\ln(Q^2) - 0.000578\ln^2(Q^2))\ln(1/x) \\ & + (0.168 + 0.138\ln(Q^2) + 0.0169\ln^2(Q^2))\ln(1/x) \end{aligned} \quad (10)$$

The gluon distribution function $G_{n_f}(x, Q^2)$ is determined by the measured $F_2(x, Q^2)$ for deep inelastic γ^*p scattering to include the effects of heavy-quark masses. Several methods for the determination of the charm and bottom quark structure functions in the nucleon have been proposed in Refs.[30-33].

The evolution equation for the proton structure function at LO approximation reads

$$\begin{aligned} \frac{1}{x} \frac{\partial F_2(x, Q^2)}{\partial \ln Q^2} = & \frac{\alpha_s}{4\pi} \left[\int_x^1 \frac{dz}{z^2} F_2(z, Q^2) K_{qq} \left(\frac{x}{z} \right) \right. \\ & \left. + \sum_i e_i^2 \frac{1}{\eta_i} \int_x^1 \frac{dz}{z^2} G(\eta_i z, Q^2) K_{gq} \left(\frac{x}{z} \right) \right], \quad (11) \end{aligned}$$

where e_i^2 is the squares of the quark charges and K 's are the splitting functions. In Eq.(11) the gluon distribution function shift from z to $\eta_i z$ for activation of heavy quarks. When taking mass effects into account, the exact solution for the gluon distribution at $n_f = 5$ has the following form

$$\begin{aligned} G(x, Q^2) = & G_{n_f=3}(x, Q^2) + \sum_{n=1}^N (-1)^n \sum_{k=0}^n \binom{n}{k} \\ & \alpha^{n-k} \beta^k G_{n_f=3}(\eta_c^{n-k} \eta_b^k x, Q^2). \quad (12) \end{aligned}$$

Here $\eta_c = 1 + 4\frac{M^2}{Q^2}$, $\eta_b = 1 + 4\frac{M^2}{Q^2}$, $\alpha = (2/3\eta_c)$, $\beta = (1/6\eta_b)$ and $\binom{n}{k}$ is a binomial coefficient. The summations in Eq.(12) are finite as the sum on n terminates at N such that $(N+1)\ln\eta_c \geq \ln(1/x)$ [28]. Indeed the

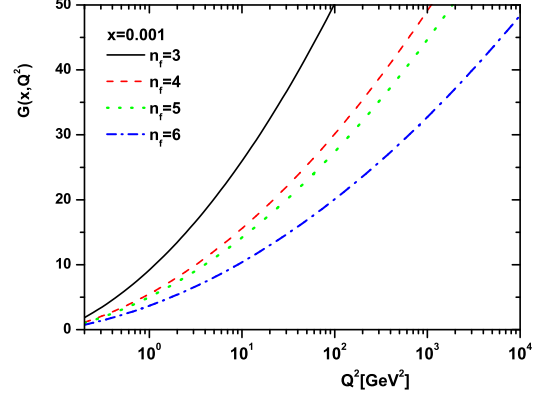


FIG. 1: The gluon distribution function at $x = 0.001$ vs. Q^2 for $n_f = \{3, 4, 5, 6\}$. $n_f = 3$ is the largest and $n_f = 6$ is the smallest curve.

ratio of the gluon distributions $\frac{G_{n_f+j}(x, Q^2)}{G_{n_f}(x, Q^2)}$, for $j = 1, 2, 3$ and $n_f = 3$, are finite by the following form

$$\frac{G_{n_f+j}(x, Q^2)}{G_{n_f}(x, Q^2)} = \frac{\sum_i^{n_f} e_i^2}{\sum_i^{n_f+j} e_i^2} \quad (13)$$

where for $j = 1, 2$ and 3 the ratio is $3/5, 6/11$ and $2/5$, respectively. Thus, the gluon distribution function for $n_f = 6$ at $Q^2 \geq m_t^2$ is obtained into the gluon distribution function of three massless quarks, $G_{n_f=3}$, by the following form

$$G_{n_f=6}(x, Q^2) = \frac{2}{5}G_{n_f=3}(x, Q^2). \quad (14)$$

This behavior of the gluon distribution function for massive c, b and t quarks [28, 34] is shown in Fig.1 over a wide range of Q^2 for $x = 10^{-3}$. In this figure (i.e., Fig.1) we display the gluon distribution function vs. Q^2 for $n_f = 3, 4, 5, 6$. We observe that the gluon distribution is reduced as a function of n_f [34]. In the following we use the massless gluon distribution functions (i.e., Eqs.(10), (8), (9) and (14)) for $n_f = 3, 4, 5, 6$ respectively as compared together in Fig.1 as the solid- black, dash-red, dot-green and dash-dot-blue curves.

Therefore, the top reduced cross section is defined as

$$\begin{aligned} \sigma_r^{t\bar{t}}(x, Q^2) = & [C_{2,g}^{t\bar{t}}(x, Q^2, m_t^2) - f(y)C_{L,g}^{t\bar{t}}(x, Q^2, m_t^2)] \\ & \otimes G_{n_f=6}(x, Q^2). \quad (15) \end{aligned}$$

With the explicit form of the coefficient functions, the top reduced cross section $\sigma_r^{t\bar{t}}(x, Q^2)$ is extracted from the parametrization of $G_{n_f}(x, Q^2)$ for $Q^2 \geq m_t^2$ in the collinear approach.

In order to make sure these results are valid in the deep inelastic region, the nonlinear corrections to the gluon

distribution is taken into account. It is known that the absorptive corrections (or gluon recombination effects) in the low x , low Q^2 region are not negligible and reduce the growth of the gluon parton distribution function. Indeed the fusion processes, $gg \rightarrow g$, for small momentum transfer in the transverse area become important [35-41]. The theoretical predictions of these effects were first emphasized long ago by Gribov, Levin and Ryskin [42] and followed by Mueller and Qiu (MQ) [43].

The evolution of the gluon density is modified at low values of x by an extra nonlinear term, quadratic in the gluon density, as

$$\frac{\partial G(x, Q^2)}{\partial \ln Q^2} = \frac{\partial G(x, Q^2)}{\partial \ln Q^2} \Big|_{DGLAP} - \frac{81}{16} \frac{\alpha_s^2(Q^2)}{\mathcal{R}^2 Q^2} \int_{\chi}^1 \frac{dz}{z} G^2\left(\frac{x}{z}, Q^2\right). \quad (16)$$

where $\chi = \frac{x}{x_0}$ and x_0 is the boundary condition that at $x \geq x_0 (= 10^{-2})$ the nonlinear corrections are negligible. The correlation length \mathcal{R} determines the size of the nonlinear terms, as $\mathcal{R} \sim 1$ is of the order of the proton radius. The \mathcal{R} is approximately equal to $\simeq 5 \text{ GeV}^{-1}$ if the gluons are populated across the proton and it is equal to $\simeq 2 \text{ GeV}^{-1}$ if the gluons have hot-spot like structure. Eq.(16) leads to saturation of the gluon density at low Q^2 with decreasing x as the nonlinear correction (NLC) to the gluon distribution is defined by the following form [44]

$$G^{\text{NLC}}(x, Q^2) = G^{\text{NLC}}(x, Q_0^2) + [G(x, Q^2) - G(x, Q_0^2)] - \int_{Q_0^2}^{Q^2} \frac{81}{16} \frac{\alpha_s^2(Q^2)}{\mathcal{R}^2 Q^2} \int_{\chi}^1 \frac{dz}{z} G^2\left(\frac{x}{z}, Q^2\right) d \ln Q^2 \quad (17)$$

where $G(x, Q^2)$ and $G(x, Q_0^2)$ are the unshadowed gluon distributions. At the initial scale Q_0^2 , the low x (i.e., $x < x_0$) behavior of the nonlinear gluon distribution is assumed to be [45]

$$G^{\text{NLC}}(x, Q_0^2) = G(x, Q_0^2) \left\{ 1 + \frac{27\pi\alpha_s(Q_0^2)}{16\mathcal{R}^2 Q_0^2} \theta(x_0 - x) \times [G(x, Q_0^2) - G(x_0, Q_0^2)] \right\}^{-1}. \quad (18)$$

In the following, the role of the nonlinear effects on the behavior of the heavy quark distribution functions in the low x region will be considered.

III. Results and Discussions

In this analysis, the value of $\alpha_s(M_z)$ is set to the world average of $\alpha_s(M_z) = 0.118$, in line with the recommended value from the particle data group (PDG) [46]. In accordance with the values recommended by

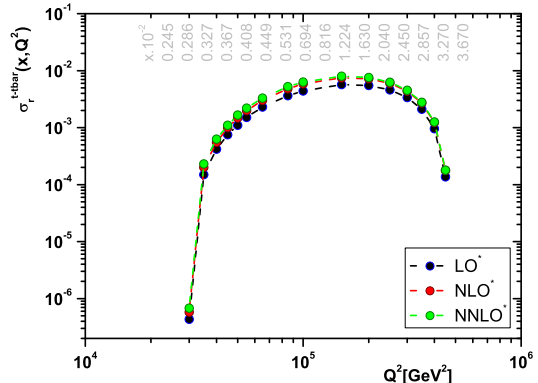


FIG. 2: The reduced top cross sections $\sigma_r^{t\bar{t}}(x, Q^2)$ plotted at different Q^2 values for $\sqrt{s} = 3.5 \text{ TeV}$ at $Q^2 \geq m_t^2$. The gray numbers on the upper scale of the figure are the Bjorken x values for each Q^2 where lie in the interval $(0.001 < x < 0.1)$. The predictions are obtained using an analytical parameterization of the gluon density at LO and the coefficient functions at LO* up to NNLO* approximations. These results represent the upper bound for top reduced cross section from the high inelasticity (i.e., $y = 1$).

the Higgs Cross Section Working Group [47], the charm-quark, bottom-quark and top-quark pole masses are set as in the NNPDF default analysis to $m_c = 1.65 \text{ GeV}$ and $m_b = 4.78 \text{ GeV}$ and $m_t = 172.5 \text{ GeV}$ [48], respectively. In Fig.2, the behavior of the top-quark reduced cross section, with respect to the number of active flavors $n_f = 6$, for $Q^2 \geq m_t^2$ at center-of-mass energy $\sqrt{s} = 3.5 \text{ TeV}$ at the high inelasticity (i.e., $y = 1$) is presented at LO up to NNLO approximations¹. In this figure we employ the LO analytic gluon distribution together with the LO up to NNLO DAS coefficient functions (in an approximately approach) in a range of the kinematical variables x and Q^2 , $x < 0.1$ (in what follows the value of $x = Q^2/sy$ for each Q^2 is provided on the upper scale of the figure) and $m_t^2 \leq Q^2 \leq 15m_t^2$. To show the contribution and importance of the longitudinal structure function $F_L^t(x, Q^2)$, the top reduced cross sections at high-inelasticity $y = 1$ are derived, as

$$\begin{aligned} \sigma_r^{t\bar{t}}(x, Q^2) &= F_2^{t\bar{t}}(x, Q^2) - F_L^{t\bar{t}}(x, Q^2), \\ &= [C_{2,g}^{t\bar{t}}(x, Q^2, m_t^2) - C_{L,g}^{t\bar{t}}(x, Q^2, m_t^2)] \\ &\quad \otimes G_{n_f}(x, Q^2). \end{aligned} \quad (19)$$

¹ The coefficient functions in our results are demonstrated in an approximation order as LO \rightarrow LO*, NLO \rightarrow NLO* and NNLO \rightarrow NNLO* for in order to distinguish these calculations from the exact calculations in LO, NLO and NNLO

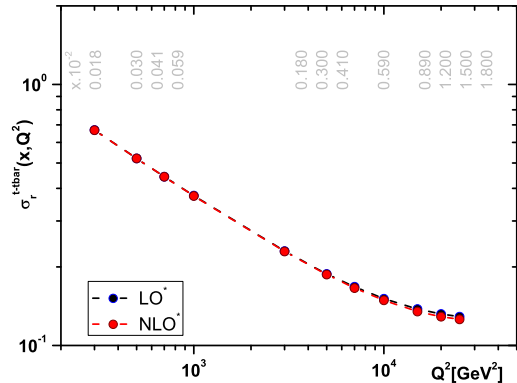


FIG. 3: The same as Fig.2 for $\sqrt{s} = 1.3$ TeV at $Q^2 < m_t^2$.

Notice that the large inelasticity is only for scattered electron energies much smaller than the electron beam energy, where the electromagnetic and hadronic backgrounds are important. Eq.(19) is an upper bound on the top reduced cross section at low x in a wide range of Q^2 . It is shown that this bound can be used to constrain the range of applicability of the linear and nonlinear corrections to the top reduced cross section at the FCC-he collider. Figure 2 clearly demonstrates that the extraction procedure provides correct behaviors of the top reduced cross section in all three, LO, NLO and NNLO approximations. In Fig.2 we observe that the maximum value for the top reduced cross section is obtained at $Q^2 \simeq 5m_t^2$. In Fig.3, the Q^2 -dependence, at low x for high inelasticity, of the top reduced cross section for $Q^2 < m_t^2$ at center-of-mass energy $\sqrt{s} = 1.3$ TeV, in the LO and NLO approximations is presented. These results determined by using the number of active flavors $n_f = 5$ which the gluon distribution corresponds to $6/11G_{n_f=3}(x, Q^2)$. In Fig.4 the top reduced cross section plotted as function of the center-of-mass energy \sqrt{s} , for the high inelasticity at the Bjorken x values $x = 0.003$ and 0.0003 . In this figure the center-of-mass energy range for the EIC to VHEeP is defined to be $100 \text{ GeV} < \sqrt{s} < 50 \text{ TeV}$. The behavior of the top reduced cross section dependence on the gluon distribution functions with respect to the number of flavors n_f as $n_f = 5$ in the region $Q^2 < m_t^2$ and $n_f = 6$ in the region $Q^2 \geq m_t^2$. Figure 5 presents the ratio $R^{t\bar{t}} = F_L^{t\bar{t}}/F_2^{t\bar{t}}$ as a function of Q^2 in a wide range of x at LO up to NNLO approximations. This shows the importance of top quark longitudinal structure function measurements [48] at energies of future ep colliders. Since the difference between the estimated $\sigma_r^{t\bar{t}}$ and $F_2^{t\bar{t}}$ is due to the contribution of the longitudinal structure function $F_L^{t\bar{t}}$, the calculations show that these contributions are rather

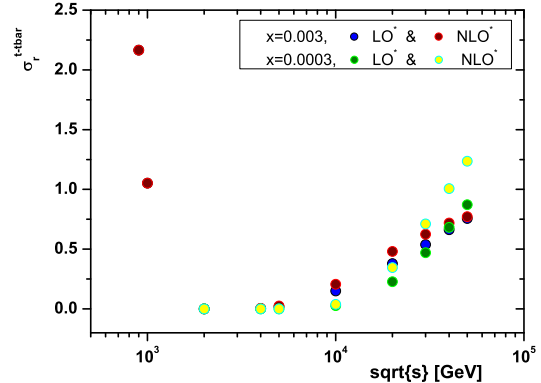


FIG. 4: The same as Fig.2 at fixed x as a function of the center-of-mass energy \sqrt{s} . The center-of-mass energy corresponding to the chosen kinematics lies in the interval $500 \text{ GeV} < \sqrt{s} \leq 50 \text{ TeV}$.

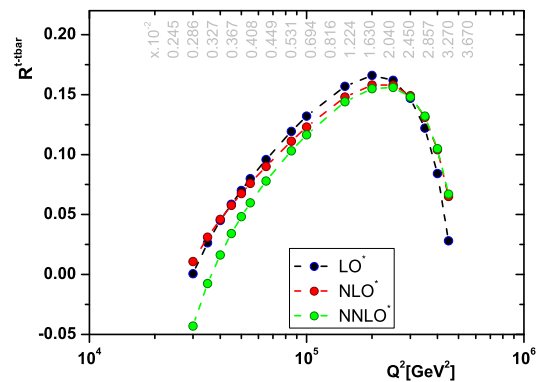


FIG. 5: The same as Fig.2 for the ratio $R^{t\bar{t}} = \frac{F_L^{t\bar{t}}}{F_2^{t\bar{t}}}$ as a function of Q^2 for $\sqrt{s} = 3.5$ TeV.

important at high Q^2 [49]. The maximum value for the ratio $R^{t\bar{t}}$ is equal to $\simeq 0.16$ for $Q^2 \simeq 5m_t^2$. For $Q^2 \gtrsim 7m_t^2$, the ratio decreases as Q^2 increases. The maximum value of the ratio $R^{t\bar{t}}$ is approximately constant [30] within the center-of-mass energy region between HERA and the FCC-he.

In Fig.6, the computed results of the nonlinear top reduced cross section are compared with the linear behavior in the LO and NLO approximations. This behavior is considered at $x < 10^{-2}$ for $Q^2 \geq m_t^2$ in the hot-spot point where the value of this parameter is defined to be $R = 2 \text{ GeV}^{-1}$ in this paper. The nonlinear effects of the top reduced cross section are very small due to the large top quark mass in a wide range of Q^2 . Consequently, knowledge of the linear and non-linear

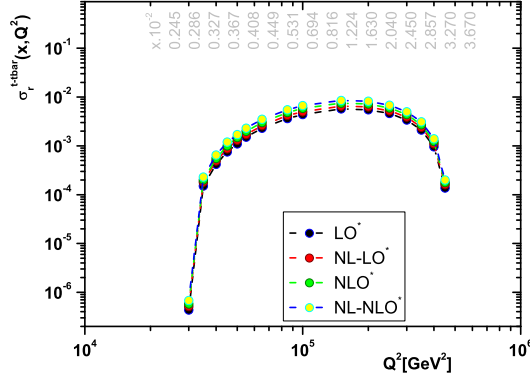


FIG. 6: The same as Fig.2 compared with the nonlinear corrections to the reduced cross section in the LO* and NLO* approximations at the hot-spot point (i.e., $R = 2 \text{ GeV}^{-1}$).

corrections offers the possibility to perform cross-section calculations of ultra-high-energy processes in heavy quark production applying higher-order corrections.

To summarize, the collinear approach to obtain the heavy-quark structure functions at small Bjorken x values in the LO up to NNLO approximations is studied. The method presents an application of extraction of the gluon density due to the number of active flavors. With respect to the parameterization of F_2 , the gluon density gives an excellent approximation behavior using a simplified ACOT approximation if the heavy-quarks are properly treated as massive. The nonlinear corrections to the heavy-quark production of gluon density at low x at hot-spot point are implemented. The heavy-quark structure functions can be improved by comparison with both experimental data and parameterization models. Above $Q^2 \geq m_t^2$, the numerical values of the top quark reduced cross section at the FCC-he collider become large in the collinear approach, which needs further investigation. For top quark pair production, which will be an important production channel at both LHeC and FCC-eh, the linear and nonlinear reduced cross sections were determined. The results of the top reduced cross section are available for high inelasticity, defined with respect to the center-of-mass energy. With this method bounds $\sigma_r^{t\bar{t}}|_{y=1}$ are derived in the collinear approach in the LO up to NNLO approximations at FCC-he center-of-mass energies. Furthermore, the importance of the longitudinal structure function measurements in top quark production at future ep collider energies are studied, investigating the ratio $F_L^{t\bar{t}}/F_2^{t\bar{t}}$. Ratios of top quark structure functions are studied in the LO up to NNLO approximations taking into account the top quark mass in the rescaling variable, which is important for the FCC-he. Furthermore, this paper proposes to perform a

study of the $t\bar{t}$ production at the high inelasticity at the future FCC-he collider.

ACKNOWLEDGMENTS

The author is thankful to the Razi University for financial support of this project. The author is especially grateful to M. Klein and C.Schwanenberger for carefully reading the paper.

APPENDIX A

In the high energy regime, defined by $x \ll 1$, the coefficient functions have the compact forms [25]

$$B_{k,g}^{(2)}(x, a) = \beta \ln(1/x) [R_{k,g}^{(2)}(1, a) + 4C_A R_{k,g}^{(1)}(1, a) L_\mu + 8C_A^2 B_{k,g}^{(0)}(1, a) L_\mu^2], \quad (20)$$

with

$$\begin{aligned} R_{2,g}^{(2)}(1, a) &= \frac{32}{27} C_A^2 [46 + (71 - 92a)J(a) + 3(13 - 10a)I(a) - 9(1 - a)K(a)], \\ R_{L,g}^{(2)}(1, a) &= \frac{64}{27} C_A^2 x_2 \{34 + 240a - [3 + 136a + 480a^2]J(a) + 3[3 + 4a(1 - 6a)]I(a) + 18a(1 + 3a)K(a)\}, \\ R_{2,g}^{(1)}(1, a) &= \frac{8}{9} C_A [5 + (13 - 10a)J(a) + 6(1 - a)I(a)], \\ R_{L,g}^{(1)}(1, a) &= -\frac{16}{9} C_A x_2 \{1 - 12a - [3 + 4a(1 - 6a)]J(a) + 12a[1 + 3a]I(a)\}, \\ B_{2,g}^{(0)}(1, a) &= \frac{2}{3} [1 + 2(1 - a)J(a)], \\ B_{L,g}^{(0)}(1, a) &= \frac{4}{3} x_2 \{1 + 6a - 4a[1 + 3a]J(a)\}, \end{aligned} \quad (21)$$

where

$$\begin{aligned} K(a) &= -\sqrt{x_2} [4(\zeta_3 + \text{Li}_3(-t)) - \text{Li}_2(-t)\ln t - 2S_{1,2}(-t) + 2\ln(ax_2)(\zeta_2 + 2\text{Li}_2(-t)) - \frac{1}{3}\ln^3 t - \ln^2(ax_2)\ln t + \ln(ax_2)\ln^2 t], \\ I(a) &= -\sqrt{x_2} [\zeta_2 + \frac{1}{2}\ln^2 t - \ln(ax_2)\ln t + 2\text{Li}_2(-t)], \\ J(a) &= -\sqrt{x_2} \ln t, \\ t &= \frac{1 - \sqrt{x_2}}{1 + \sqrt{x_2}}, \\ x_2 &= \frac{1}{1 + 4a}, \\ L_\mu &= \ln \frac{4m^2}{\mu^2}, \end{aligned} \quad (22)$$

where

$$\begin{aligned}
 \text{Li}_2(x) &= -\int_0^1 \frac{dy}{y} \ln(1-xy), \\
 \text{Li}_3(x) &= -\int_0^1 \frac{dy}{y} \ln(y) \ln(1-xy), \\
 S_{1,2}(x) &= \frac{1}{2} \int_0^1 \frac{dy}{y} \ln^2(1-xy),
 \end{aligned}
 \tag{23}$$

are the dilogarithmic function $\text{Li}_2(x)$, the trilogarithmic function $\text{Li}_3(x)$ and Nielsen Polylogarithm $S_{1,2}(x)$.

References

1. P.Agostini et al. [LHeC Collaboration and FCC-he Study Group], J. Phys. G: Nucl. Part. Phys. **48**, 110501 (2021).
2. A. Abada et al., [FCC Collaboration], Eur.Phys.J.C **79**, 474 (2019).
3. M.Klein, arXiv:1802.04317; Annalen Phys. **528**, 138(2016).
4. R.A.Khalek et al., SciPost Phys.**7**, 051(2019).
5. A. Caldwell and M. Wing, Eur. Phys. J. C **76**, 463 (2016); A. Caldwell, et al., arXiv:1812.08110.
6. G. R. Boroun, ; Phys.Lett.B **744**, 142 (2015); Phys.Lett.B **741**, 197 (2015); Physics of Particles and Nuclei Letters **15**, 387(2018); Chin.Phys. C **41**, 013104 (2017).
7. I. A. Sarmiento-Alvarado, A. O. Bouzas, and F. Larios, J. Phys. G **42**, 085001 (2015).
8. Turk Cakir, A. Yilmaz, H. Denizli, A. Senol, H. Karadeniz, and O. Cakir, Adv. High Energy Phys.**2017**, 1572053 (2017).
9. H. Sun (LHeC/FCC-eh top physics Study Group), PoS DIS2018, 186 (2018).
10. C. Schwanenberger, PoS EPS-HEP2019, 635 (2020).
11. W. Liu and H. Sun, Phys. Rev. D **100**, 015011 (2019); B. Yang, B. Hou, H. Zhang, and N. Liu, Phys. Rev. D **99**, 095002 (2019); B. Rezaei and G. R. Boroun, EPL **130**, 51002 (2020).
12. H.Khanpour, Nucl.Phys.B **958**, 115141 (2020).
13. G.R.Boroun and B.Rezaei, EPL **133**, 61002 (2021).
14. M.Gao and J.Gao, Phys. Rev. D **104**, 053005 (2021).
15. V.A.Okorokov, J. Phys.: Conf. Ser. 1690, 012006, (2020).
16. O.B.Bylund, arXiv:2103.14772.
17. E.R.Nocera, M.Ubiali and C.Voisey, JHEP **05**, 067 (2020).
18. P.A.Zyla, et al. (Particle Data Group) (2020) Review of Particle Physics. Progress of Theoretical and Experimental Physics, 2020, 083C01.
19. CMS Collaboration, Eur.Phys.J.C **79**, 368 (2019); Phys. Rev. D **93**, 072004 (2016); ATLAS Collaboration, Phys. Lett. B **810**, 135797(2020); Eur. Phys. J. C **79**, 290 (2019).
20. Tie-Jiun Hou et al., Phys.Rev.D**103**, 014013(2021).
21. R.S.Thorne, arXiv:hep-ph/9805298(1998).
22. A.D.Martin W.J.Stirling and R.S.Thorne, Phys.Lett.B **636**, 259(2006).
23. J.Blümlein, A.De Freitas, C.Schneider and K.Schönwald, Phys. Lett.B **782**, 362(2018).
24. S.Alekhin, J. Blümlein and S. Moch, Phys. Rev. D **102**, 054014 (2020).
25. A.V.Kotikov, A.V.Lipatov and P.Zhang, Phys. Rev. D **104**, 054042 (2021).
26. M.A. Kimber, A.D. Martin, M.G. Ryskin, Phys. Rev. D **63**, 114027 (2001); G. Watt, A.D. Martin, M.G. Ryskin, Eur. Phys. J. C **31**, 73 (2003).
27. A.V. Kotikov, G. Parente, Nucl. Phys. B **549**, 242 (1999); A.Yu. Illarionov, A.V. Kotikov, G. Parente, Phys. Part. Nucl. **39**, 307 (2008); L. Mankiewicz, A. Saalfeld, T. Weigl, Phys. Lett. B **393**, 175 (1997).
28. M.M.Block and L.Durand, arXiv: 0902.0372 [hep-ph](2009); E.L. Berger, M.M. Block and Chung-I Tan, Phys.Rev.Lett. **98**, 242001 (2007); M.M. Block, L. Durand and D.W. McKay, Phys.Rev.D **79**, 014031 (2009).
29. M.A.G.Aivazis, J.C.Collins, F.I.Olness and W.-K.Tung, Phys.Rev.D **50**, 3102 (1994).
30. A.Y.Illarionov, B.A.Kniehl and A.V.Kotikov, Phys.Lett.B **663**, 66 (2008); A.Y.Illarionov and A.V.Kotikov, Phys.Atom.Nucl **75**, 1234 (2012).
31. G.R.Boroun and B.Rezaei, Int.J.Mod.Phys.E **24**, 1550063(2015); Nucl.Phys.A **929**, 119(2014); EPL **100**, 41001(2012); J.Exp.Theor.Phys. **115**, 427(2012); Nucl.Phys.B **857**, 143(2012).
32. J.Lan et al., Phys. Rev. D **102**, 014020 (2020); N.N.Nikolaev and V.R.Zoller, Phys.Atom.Nucl. **73**, 672(2010); A. V. Kotikov, A. V. Lipatov, G. Parente and N. P. Zotov, Eur. Phys. J. C **26**, 51 (2002).
33. G.R.Boroun, Nucl.Phys.B **884**, 684(2014).
34. D.B.Clark, E.Godat and F.I.Olness, Comput.Phys.Commun. **216**, 126 (2017).
35. A.V.Giannini and F.O.Durães, Phys.Rev.D **88**, 114004(2013).
36. G.R.Boroun and B.Rezaei, Phys. Rev. C **103**, 065202 (2021).
37. R.Wang and X.Chen, Chinese Phys.C **41**, 053103(2017).
38. G.R.Boroun and S.Zarrin, Eur.Phys.J.Plus **128**, 119(2013).
39. B.Rezaei and G.R.Boroun, Phys.Lett.B **692**, 247(2010).
40. D. Britzger, C. Ewerz, S. Glazov, O. Nachtmann, and S. Schmitt, Phys. Rev. D **100**, 114007 (2019).
41. G.R.Boroun, Eur.Phys.J.A **42**, 251(2009); Eur.Phys.J.A **43**, 335(2010).
42. L. V. Gribov, E. M. Levin and M. G. Ryskin, Phys.

- Rep. **100**, 1 (1983).
43. A. H. Mueller and Jianwei Qiu, Nucl. Phys. B **268**, 427 (1986).
44. G.R.Boroun and B.Rezaei, Eur.Phys.J.C **81**, 851 (2021); A.V. Kotikov, JETP Lett. **111**, 67 (2020).
45. J.Kwiecinski et al., Phys.Rev.D **42**, 3645 (1990).
46. PARTICLE DATA GROUP collaboration, *Review of particle physics*, Phys.Rev.D **98**, 030001 (2018).
47. LHC Higgs Cross Section Working Group collaboration, arXiv:1610.07922.
48. NNPDF Collaboration (Ball R. D. et al.), Eur. Phys. J. C **77**, 663 (2017).
49. G. R. Boroun, Chin. Phys. C **45**, 063105 (2021).